

Coherent vorticity extraction in turbulent boundary layers using orthogonal wavelets

By George Khujadze[†], Romain Nguyen van yen[‡], Kai Schneider[¶],
Martin Oberlack^{†||††}, Marie Farge[‡]

High-resolution data obtained by direct numerical simulation of turbulent boundary layers are analysed by means of orthogonal wavelets. The data, originally given on a Chebychev grid, are first interpolated onto an adapted dyadic grid. Then, they are decomposed using a wavelet basis, which accounts for the anisotropy of the flow by using different scales in the wall-normal direction and in the planes parallel to the wall. Thus the vorticity field is decomposed into coherent and incoherent contributions using thresholding of the wavelet coefficients. It is shown that less than 1% of the coefficients retain the coherent structures of the flow, while the majority of the coefficients corresponds to a structureless, *i.e.*, noise-like background flow. Scale- and direction-dependent statistics in wavelet space quantify the flow properties at different wall distances.

1. Introduction

This study is motivated by the importance of turbulent boundary layers in many fields of applied physics, for example, flows around technological devices such as airplanes, cars or golf balls, where determining the drag coefficient is directly related to this thin layer around the obstacle. In geophysical flows, the atmospheric boundary layer also plays a prevailing role. For a review on the subject we refer the reader to the classical textbook by Schlichting & Gersten (2003). Direct numerical simulations of turbulent boundary layers are still a challenging problem and constitute a major challenge in computational fluid dynamics for both numerical discretization schemes and computer resources. The stiffness is due to the very high resolution which is required to resolve all dynamically active scales of the flow. Spalart (1988) did the first numerical simulations of turbulent boundary layers. Over the past several years, a number of simulations of such flows for higher Reynolds numbers have become available (see Skote (2001); Khujadze & Oberlack (2004, 2007); Simens *et al.* (2009); Schlatter *et al.* (2009)). One important research subject is the identification and extraction of coherent structures in turbulent boundary layers. This is inspired by the existence of horseshoe vortices first observed by Theodorsen (1952). The observation of forests of horseshoe vortices in experimental data by Adrian *et al.* (2000) and in direct numerical simulations (DNS) recently performed by Wu & Moin (2009) gave a second wind to this topic.

Wavelet techniques have been developed for more than 20 years (see, *e.g.*, Farge (1992) for an early review) to analyse, model, and compute turbulent flows. The multiscale representation obtained by wavelet decompositions is useful in understanding the physics of

[†] Chair of Fluid Dynamics, TU Darmstadt, Petersenstr. 30, 64287 Darmstadt, Germany

[‡] LMD-IPSL-CNRS, Ecole Normale Supérieure, 24 rue Lhomond, 75231 Paris Cedex 5, France

[¶] M2P2-CNRS & CMI Université de Provence, 39 rue Joliot-Curie, 13453 Marseille Cedex 13, France

^{||} Center of Smart Interfaces, TU Darmstadt, Petersenstr. 32, 64287 Darmstadt, Germany

^{††} GS Computational Engineering, TU Darmstadt, Dolivostr. 15, 64293 Darmstadt, Germany

turbulent flows as locality in both space and scale is preserved. Thus localised features of turbulent flows, such as coherent structures and intermittency can be extracted and analysed. Coherent Vorticity Extraction (CVE) has been introduced for two- and three-dimensional turbulent flows in Farge *et al.* (1999) and Farge *et al.* (2001), respectively. The underlying idea is that coherent structures are defined as what remains after denoising and hence only a hypothesis on the noise has to be made. In the present study we assume the noise to be Gaussian and white. Preliminary results of CVE applied to wall-bounded flows, for a channel flow, have been reported in Weller *et al.* (2006). Scale-dependent and directional statistics in wavelet space have been presented in Bos *et al.* (2007) to quantify the intermittency of anisotropic flows. Mixing layers have been analysed in Schneider *et al.* (2005) and sheared and rotating flows more recently in Jacobitz *et al.* (2010). An up-to-date review on wavelet techniques in computational fluid dynamics can be found in Schneider & Vasilyev (2010).

In the present paper we apply orthogonal wavelet analysis for the first time to new DNS data of three-dimensional turbulent boundary layers computed with the code of KTH (Lundbladh *et al.* (1999)) for higher Reynolds numbers as published in Khujadze & Oberlack (2004, 2007). Additional difficulties are encountered due to the non-equidistant grid in the wall-normal direction. The aim of this paper is to extract coherent structures out of high-resolution DNS of zero-pressure-gradient turbulent boundary layer flow at $Re_\theta = 1470$. The vorticity of the flow is decomposed into coherent and incoherent parts and scale-dependent statistics, *i.e.*, variance, flatness and probability distribution functions, are computed at different wall-normal positions. These analyses are only a first step as they are limited to flow snapshots. A detailed investigation of the dynamics of the coherent and incoherent flow contributions is left for future work.

The paper is organised as follows. Section 2 presents the flow configuration and the computational approach. Some visualisation and analyses of the DNS data are also given. The CVE methodology is described in Section 3, mentioning technical details like the required interpolation on a dyadic adapted grid, the adaptive anisotropic wavelet transform and the wavelet-based statistics which are applied in the numerical results in Section 4. The latter discusses the total, coherent, and incoherent flows using both flow visualisation and statistical analyses. The efficiency of CVE is also assessed. Finally, conclusions are drawn in Section 5 and some perspectives for future investigations are given.

2. Flow configuration and parameters

Here we give some details on the DNS code for solving the incompressible Navier–Stokes equations which was developed at KTH, Stockholm; for details we refer the reader to Lundbladh *et al.* (1999). A spectral method with a Fourier decomposition is used in the horizontal directions, while a Chebyshev discretization is applied in the wall-normal direction. Third-order explicit Runge-Kutta and Crank-Nicolson schemes were used for the time integration for the advective and the viscous terms correspondingly. Since the boundary layer is developing in the downstream direction, a fringe region (where the outflow is forced by a volume force to the laminar inflow Blasius profile) has to be added to the physical domain to satisfy the periodic boundary condition. A wall-normal trip force is used to trigger the transition to turbulence. Since the first study by Spalart (1988), several other authors have also used this approach for simulating zero-pressure-gradient (ZPG) turbulent boundary layer flows. Note that it assumes that the boundary layer thickness remains sufficiently small in the whole computational domain. Extensive

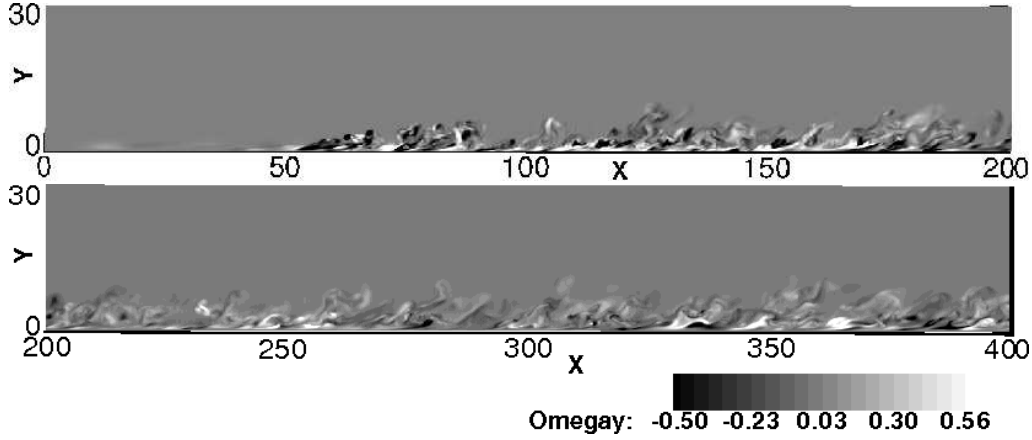


FIGURE 1. Two-dimensional slices of ω_y at $z = 0$ for $x \in [0, 200]$ (top) and for $x \in [200, 400]$ (bottom).

studies of turbulent boundary layer flows were performed by Skote (2001). Here we give some details about the simulations used in our study. DNS of ZPG turbulent boundary layer flow was performed for a number of grid points $N_x \times N_y \times N_z = 2048 \times 513 \times 256$ at starting laminar Reynolds number $Re_{\delta^*}|_{x=0} \equiv \frac{u_\infty \delta^*|_{x=0}}{\nu} = 600$. All quantities were non-dimensionalized by the free-stream velocity u_∞ and the displacement thickness δ^* at $x = 0$, where the flow is laminar. The size of the computational box was $L_x \times L_y \times L_z = 1000 \delta^*|_{x=0} \times 30 \delta^*|_{x=0} \times 34 \delta^*|_{x=0}$. Figure 1 represents only part of the computational domain, *i.e.*, for $0 \leq x \leq 400$. The axes x, y and z correspond to the streamwise, wall-normal, and spanwise directions respectively. The flow is assumed to extend to an infinite distance perpendicular to the wall. However, the discretization used in the code can only handle a finite domain size. Therefore, the flow domain is truncated and an artificial boundary condition is applied in the freestream at the wall-normal position y_L . In the present computations we use a generalisation of the boundary condition introduced by Malik *et al.* (1985) which allows the boundary to be placed closer to the wall. The boundary condition exactly represents a potential flow solution decaying away from the wall. It is essentially equivalent to requiring that the vorticity is zero at the boundary. Thus, it can be applied immediately outside the vortical part of the flow.

The simulations were run for a total of 11500 time units ($\delta^*|_{x=0}/u_\infty$). The range of Reynolds numbers was $Re_\theta \approx 500$ -1470 with $Re_\theta = \frac{u_\infty \theta}{\nu}$ and where θ is the momentum loss thickness. The grid resolution in viscous or plus units ($\Delta x^+ \equiv \Delta x/u_\tau \nu$, where u_τ is the friction velocity) was $\Delta x^+ \times \Delta y^+ \times \Delta z^+ = 12.8 \times (0.018 \text{ to } 5) \times 3.5$.

Figure 2 (left) shows the mean velocity profile in lin-log representation. The dashed line corresponds to the fit of the classical log-law and the solid line represents the present DNS at $Re_\theta = 1470$. The fit shows that for $3 < y^+ < 20$ the DNS mean velocity exhibits a log-law. A comparison of the normal Reynolds stresses between our and those data of Simens *et al.* (2009) is given in Figure 2 (right), which shows a reasonable agreement.

3. Orthogonal wavelet decomposition of the turbulent boundary layer flow

In the following we introduce a new anisotropic wavelet decomposition with an adaptive grid in the wall-normal direction which allows for analysis of the DNS data. Then, the

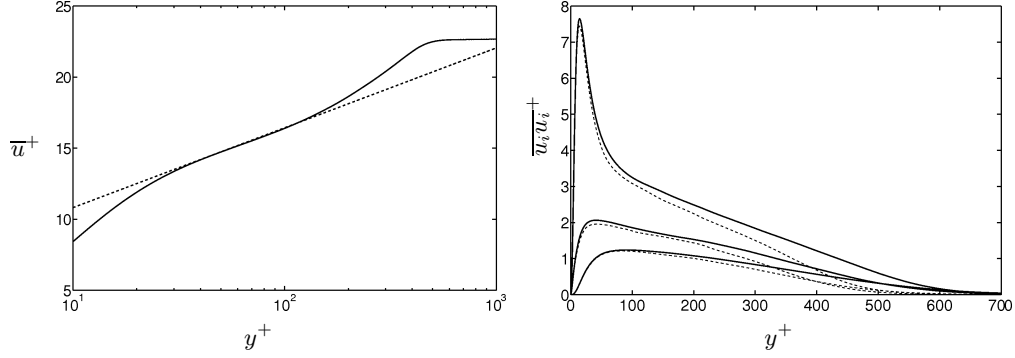


FIGURE 2. *Left plot*: Mean velocity profile in lin-log representation at $Re_\theta = 1470$. --- $1/\kappa \log y^+ + B$ with $\kappa = 0.41$ and $B = 5.2$; *Right plot*: Diagonal components of Reynolds stress tensor for the present DNS (---) and from Simens *et al.* (2009) (—) at the $Re \approx 1550$, with $\overline{u_1 u_1}^+ > \overline{u_3 u_3}^+ > \overline{u_2 u_2}^+$.

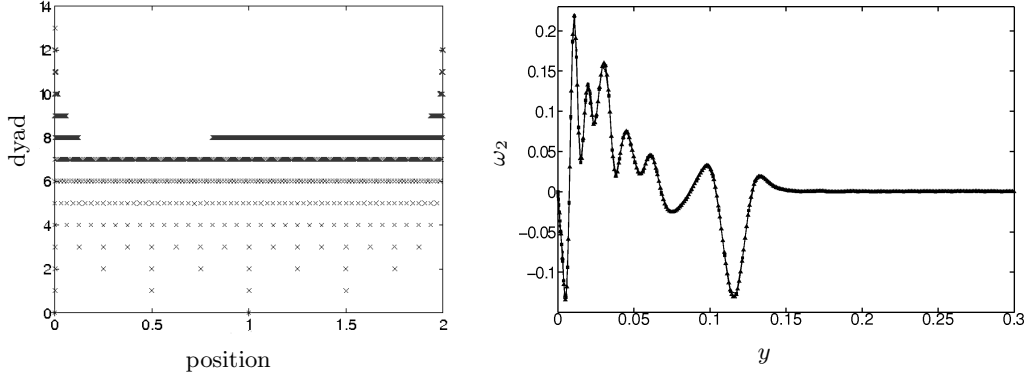


FIGURE 3. *Left plot*: Adapted dyadic grid by the position of the corresponding wavelets. *Right plot*: Interpolation of vorticity ω_y in the wall-normal direction. \square — Original/Chebyshev grid, \triangle — dyadic grid, \times — reinterpolated on Chebyshev grid.

coherent vorticity extraction is presented and different scale-dependent wavelet based statistics are described.

3.1. Adaptive anisotropic wavelet decomposition

From the velocity field $\mathbf{u} = (u_1, u_2, u_3)$ we compute the vorticity field $\boldsymbol{\omega} = (\omega_1, \omega_2, \omega_3) = \nabla \times \mathbf{u}$. Both fields are given on discrete grid points (x_i, y_n, z_k) for $i = 1, \dots, N_x$, $n = 1, \dots, N_y$, and $k = 1, \dots, N_z$. The grid is equidistant in the wall-parallel directions x and z , while in the wall-normal direction y a Chebyshev grid is used, *i.e.*, $y_n = \cos(\pi\theta_n)$ with $\theta_n = (n-1)/(N_y-1)$ for $n = 1, \dots, N_y$, and rescaled to $(0, L_y)$.

Each component ω_ℓ of the vorticity vector is then decomposed into a two-dimensional orthogonal wavelet series in the wall-parallel directions x - z using a two-dimensional multiresolution analysis. The number of scales J_{xz} is defined as the maximum integer such that $N_x = k2^{J_{xz}}$ and $N_z = k'2^{J_{xz}}$ where k and k' are any integers. For a fixed wall-normal position y_n we thus obtain for $\ell = 1, 2, 3$,

$$\omega_\ell(x, y_n, z) = \sum_{j_{xz}=0}^{J_{xz}-1} \sum_{i_x=0}^{2^{J_{xz}}-1} \sum_{i_z=0}^{2^{J_{xz}}-1} \sum_{\mu=1}^3 \langle \omega_\ell(y_n), \psi_{j_{xz}, i_x, i_z}^\mu \rangle_{xz} \psi_{j_{xz}, i_x, i_z}^\mu(x, z), \quad (3.1)$$

with the wavelet

$$\psi_{j_{xz}, i_x, i_z}^\mu(x, z) = \begin{cases} \psi_{j_{xz}, i_x}(x)\phi_{j_{xz}, i_z}(z) & \text{for } \mu = 1 \\ \phi_{j_{xz}, i_x}(x)\psi_{j_{xz}, i_z}(z) & \text{for } \mu = 2 \\ \psi_{j_{xz}, i_x}(x)\psi_{j_{xz}, i_z}(z) & \text{for } \mu = 3 \end{cases} \quad (3.2)$$

where ϕ and ψ are the one-dimensional scaling function and wavelet, respectively, and $\mu = 1, 2$ and 3 corresponds to the direction of wavelets in the x , z and xz direction, respectively. The scalar product is defined in the x - z plane, $\langle f, g \rangle_{xz} = \int f(x, z)g(x, z)dx dz$. Here we use Coiflet 12 wavelets (see *e.g.* Farge 1992) and the scaling coefficients on the finest scale are identified with the grid point values.

Before performing a one-dimensional wavelet transform in the y -direction (while fixing the x - z direction), the vorticity components ω_ℓ have to be interpolated from the Chebyshev grid onto a locally refined dyadic grid. For that a Lagrange interpolation of 4-th order is used and a Haar wavelet transform is applied to the Chebyshev grid $\arccos(y_n)$ to define the locally refined dyadic grid $\tilde{y}_n = i_y/2^{j_y}$ (rescaled to $[0, 1]$) for $j_y = 0, \dots, J_y - 1$ and $i_y = 0, \dots, 2^{j_y} - 1$ using nonlinear approximation. The number of grid points in the y -direction is fixed, here to $\tilde{N}_y = 1024$. The maximal scale in y -direction, J_y , is then determined from the Haar wavelet analysis retaining the \tilde{N}_y strongest coefficients. In the present case we obtain $J_y = 13$. The resulting dyadic grid is shown in Figure 3 (left) which yields the best approximation of the Chebyshev grid using a dyadic grid with $\tilde{N}_y = 1024$ grid points. The one-dimensional vorticity cuts in the y -direction in Figure 3 (right) show the original data on the Chebyshev grid, the data interpolated onto the refined dyadic grid and after reinterpolation onto the Chebyshev grid. The agreement between the curves is satisfactory and thus we can conclude that the interpolation between the different grids can be performed with little loss of information.

A wavelet decomposition using Daubechies 4 wavelets (Farge 1992) is then applied to the data on the adaptive dyadic grid and the scaling coefficients at the finest scale are computed using a quadrature rule. Thereafter an adaptive wavelet transform is performed on the adaptive dyadic grid and we obtain a full wavelet decomposition in all three space directions,

$$\omega_\ell(x, y, z) = \sum_{j_{xz}=0}^{J_{xz}-1} \sum_{j_y=0}^{J_y-1} \sum_{i_x=0}^{2^{j_{xz}}-1} \sum_{i_y=0}^{2^{j_y}-1} \sum_{i_z=0}^{2^{j_{xz}}-1} \sum_{\mu=1}^3 \tilde{\omega}_{j_{xz}, j_y, i_x, i_y, i_z}^{\ell, \mu} \psi_{j_{xz}, i_x, i_z}^\mu(x, z) \psi_{j_y, i_y}(y) \quad (3.3)$$

for $\ell = 1, 2, 3$. Note that the wavelet coefficients

$$\tilde{\omega}_{j_{xz}, j_y, i_x, i_y, i_z}^{\ell, \mu} = \int \int \int \omega_\ell(x, y, z) \psi_{j_{xz}, i_x, i_z}^\mu(x, z) dx dz \psi_{j_y, i_y}(y) dy$$

contain different scales in the wall-parallel (x - z) and the wall normal (y) direction. This property allows to take into account the anisotropy of the structures observed in the DNS data.

3.2. Coherent vorticity extraction

The starting point of the coherent vorticity extraction is the wavelet representation of vorticity in Eq. (3.3). The underlying idea is to perform denoising of vorticity in wavelet coefficient space. Thresholding the wavelet coefficients then determines which coefficients belong to the coherent and to the incoherent contributions. The latter are assumed to be noise-like. First we compute $\Omega = \left(\sum_{\ell=1}^3 \left(\tilde{\omega}_{j_{xz}, j_y, i_x, i_y, i_z}^{\ell, \mu} \right)^2 \right)^{1/2}$ and then we reconstruct

the coherent vorticity ω_c from those wavelet coefficients for which $\Omega > \epsilon$ using Eq. (3.3). The incoherent vorticity ω_i is obtained from the remaining weak wavelet coefficients. In the first iteration the threshold ϵ is determined from the total enstrophy $Z = \frac{1}{2} \langle \omega \cdot \omega \rangle_{xyz}$ and the total number of grid points $N = N_x \tilde{N}_y N_z$, *i.e.*, $\epsilon = \sqrt{4Z \ln N}$. Subsequently, a new threshold is determined using the incoherent enstrophy computed from the weak wavelet coefficients instead of the total enstrophy. Then the thresholding is applied again and improved estimators of the coherent and incoherent vorticities are obtained. For more details on the iterative procedure we refer to Farge *et al.* (1999). We note that thanks to the orthogonality of the decomposition, the enstrophy and thus the threshold can be directly computed in coefficient space using Parseval's relation. Only at the end of the iterative procedure are the coherent and incoherent vorticities reconstructed by inverse wavelet transform in physical space, in the x - z direction on a regular grid and in the y direction on the locally refined dyadic grid. Afterwards the vorticity fields are reinterpolated in y -direction onto the Chebyshev grid.

Finally, we thus obtain $\omega = \omega_c + \omega_i$ and by construction we also have $Z = Z_c + Z_i$. For future work we anticipate that the corresponding velocity fields can also be reconstructed by applying Biot-Savart's kernel, which necessitates the solution of three Poisson equations.

3.3. Scale-dependent statistics

The wavelet-based scale-dependent statistics are built on the two-dimensional wavelet representation (Eq. 3.1) for a fixed position in the wall-normal direction y_n . First we define the scale-dependent p -th order moments of the three vorticity components ω_ℓ in wavelet coefficient space by

$$M_{j_{xz}}^{p,\ell}(y_n) = \sum_{i_x=0}^{2^{j_{xz}}-1} \sum_{i_z=0}^{2^{j_{xz}}-1} (\langle \omega_\ell(y_n), \psi_{j_{xz},i_x,i_z}^\mu \rangle_{xz})^p . \quad (3.4)$$

The scale-dependent variance of the vorticity components corresponds to $p = 2$. Dividing it by two the scalogram of enstrophy is obtained, which yields a scale distribution of enstrophy for a given position y_n . Scale-dependent flatness of each vorticity component ω_ℓ can be defined as

$$\mathcal{F}_{j_{xz}}^\ell(y_n) = \frac{M_{j_{xz}}^{4,\ell}(y_n)}{\left(M_{j_{xz}}^{2,\ell}(y_n)\right)^2} . \quad (3.5)$$

Note that for Gaussian statistics the flatness equals three on all scales. The flatness (Eq. 3.5) quantifies the intermittency of the flow and is directionally related to spatial fluctuations in the x - z plane of the enstrophy. Indeed, as shown in Bos *et al.* (2007), increasing flatness values for finer scale are an indicator of intermittency.

Finally, we also consider the probability distribution functions (pdfs) of the wavelet coefficients at given scale j_{xz} and wall-normal position y_n estimated by histograms using 128 bins. As the number of wavelet coefficients decreases at each larger scale by a factor 4, we only consider the last three scales $j_{xz} = 6, 7, 8$ in order to have sufficient statistics.

4. Numerical results

Visualisations of the modulus of vorticity $|\omega|$ are shown in Figure 4 for the total (top), coherent (middle) and incoherent contributions (bottom). It can be observed that the

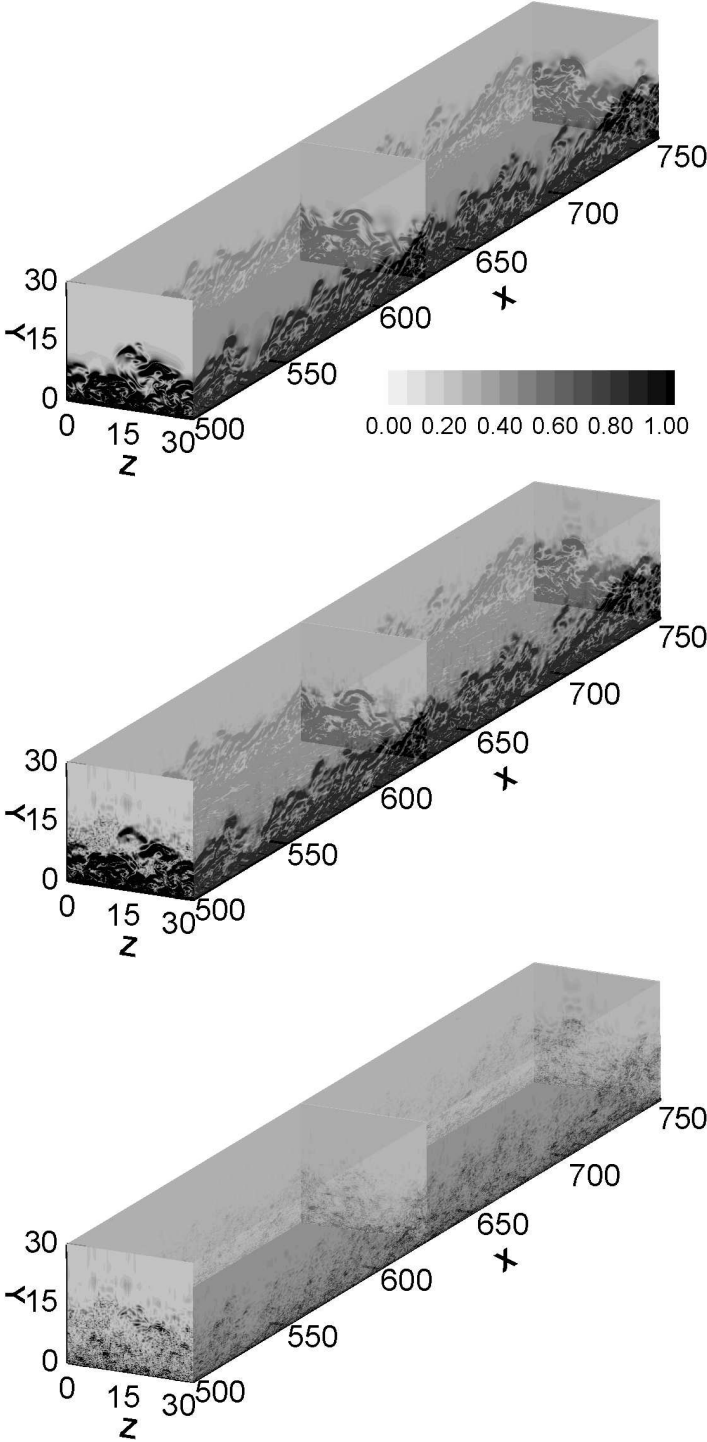


FIGURE 4. Visualisation of the modulus of vorticity $|\omega|$ for the analysed subdomain $[500, 750] \times [0, 60] \times [0, 34]$. The visualisations show a zoom for $y \in [0, 30]$: total (top), coherent (middle), and incoherent contributions (bottom).

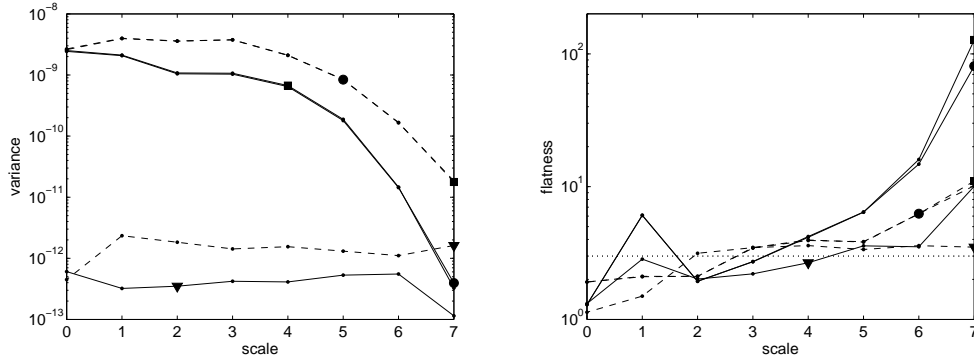


FIGURE 5. Scale-dependent second-order moments (left) and scale-dependent flatness (right) of the vorticity component ω_z for the total (circles), coherent (squares) and incoherent (triangles) flows at two different wall distances, $y^+ = 30$ (—) and $y^+ = 153$ (---).

coherent vortices present in the total field are well preserved in the coherent field using only 0.84 % of the total number of wavelet coefficients $N_x \tilde{N}_y N_z$, which retain 99.61% of the total enstrophy of the flow. In contrast, the incoherent vorticity field has weaker amplitude and is almost structureless.

The statistics of the different flow contributions are quantified in Figure 5 by considering the second-order moments and the flatness as a function of scale of the vorticity component ω_z for the total, coherent, and incoherent flows at two different wall distances, at $y^+ = 30$, which is at the beginning of the log-layer and at $y^+ = 153$, which is inside the log-layer. The variance illustrates the good agreement between the total and coherent vorticity, while the variance of the incoherent one is more than three orders of magnitude smaller. The latter also only weakly depends on scale, which indicates an equipartition of enstrophy and thus confirms that the incoherent part is close to white noise. The flatness for both the total and coherent vorticity increases with scale, which is a signature of intermittency. The flatness of the incoherent part features values around 3, which is characteristic for Gaussian noise. The probability distribution functions of the wavelet coefficients at scales $j_{xz} = 6$ and 7 are plotted in Figure 6 at two different wall distances. Close to the wall, for $y^+ = 30$, we observe an algebraic decay of the pdf tails with slope -2 , which is close to a Cauchy distribution and corresponds to strong intermittency. For distances further away from the wall, $y^+ = 153$, the tails of the pdf become exponential which shows that the flow becomes less intermittent. We can also observe that the pdfs do not differ much for the two scales considered here.

5. Conclusions and perspectives

A zero-pressure-gradient three-dimensional turbulent boundary layer was studied by means of high-resolution DNS at $Re_\theta = 1470$. The flow data were shown to be in agreement with previous DNS results by Simens *et al.* (2009) and visualisations gave some evidence for the existence of horseshoe vortices.

A new adaptive three-dimensional wavelet transform was developed which accounts for the flow anisotropy by using different scales in the wall-normal and wall-parallel directions. Coherent vorticity extraction was applied and the obtained results showed that fewer wavelet coefficients ($< 1\%N$) are sufficient to retain the coherent flow structures, while the large majority of coefficients corresponds to the incoherent background

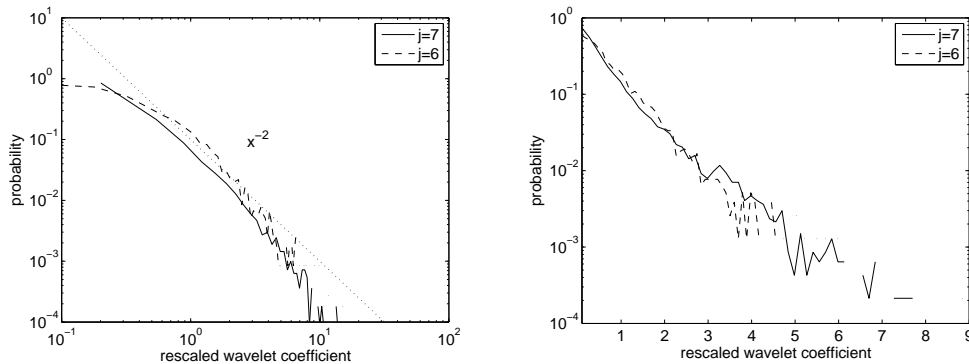


FIGURE 6. Probability distribution functions of the wavelet coefficients of ω_z in the xz -plane at scales $j_{xz} = 6$ and 7 estimated by histograms using 128 bins at two different wall distances, $y^+ = 30$ (left) and $y^+ = 153$ (right).

flow which is unstructured and noise-like. Scale-dependent statistics quantified the total, coherent and incoherent flows for different wall-normal positions and showed that the statistics of the total and coherent flows are in good agreement. The scale-dependent flatness allowed the flow intermittency at different wall distances to be quantified and showed that, in contrast to the total and coherent flows, the incoherent flow is Gaussian like.

The current work is limited to time snapshots of vorticity. The reconstruction of the velocity fields from the total, coherent, and incoherent vorticity is a prerequisite to perform dynamical analyses of the flow, such as determining the energy transfer between the different flow contributions. In future work we plan to rerun three simulations initialised with either the total, coherent or incoherent flow and to compare their dynamics. On a longer term perspective we also envisage performing Coherent Vorticity Simulation of turbulent boundary layer flows by advancing only the coherent contributions in time.

GK and MO gratefully acknowledge funding from Deutsche Forschungsgemeinschaft (DFG) under grant number OB 96/13-2. GK, MO and KS acknowledge financial support and hospitality from the Center for Turbulence Research, Stanford University/NASA Ames, during the summer program 2010. MF and KS gratefully acknowledge financial support from the ANR, project M2TFP and MF thanks the Wissenschaftskolleg zu Berlin. RNY, KS and MF are grateful to CNRS supporting their work under a contract PEPS-INSMI-CNRS.

REFERENCES

- ADRIAN, R.J., MEINHART, C.D. & TOMKINS, C.D. 2000 Vortex organization in the outer region of the turbulent layer. *J. Fluid Mech.* **422**, 1–54.
- BOS, W.J.T., LIECHTENSTEIN, L. & SCHNEIDER, K. 2007 Small scale intermittency in anisotropic turbulence. *Phys. Rev. E* **76**, 046310.
- FARGE, M. 1992 Wavelet transforms and their applications to turbulence. *Annu. Rev. Fluid Mech.* **24**, 395.
- FARGE, M., PELLEGRINO, G. & SCHNEIDER, K. 2001 Coherent vortex extraction in 3D turbulent flows using orthogonal wavelets. *Phys. Rev. Lett.* **87** (5), 45011–45014.

- FARGE, M., SCHNEIDER, K. & KEVLAHAN, N. 1999 Non-Gaussianity and coherent vortex simulation for two-dimensional turbulence using an adaptive orthonormal wavelet basis. *Phys. Fluids* **11** (8), 2187–2201.
- JACOBITZ, F., SCHNEIDER, K., BOS, W.J.T. & FARGE, M. 2010 On the structure and dynamics of sheared and rotating turbulence: Anisotropy properties and geometrical scale-dependent statistics. *Phys. Fluids* **22**, 085101.
- KHUJADZE, G. & OBERLACK, M. 2004 DNS and scaling laws from new symmetry groups of ZPG turbulent boundary layer flow. *Theor. Comput. Fluid Dyn.* **18**, 391–411.
- KHUJADZE, G. & OBERLACK, M. 2007 New scaling laws in ZPG turbulent boundary layer flow. In *Proceedings of 5th Int. Symp. on Turbul. Shear Flow Phenom.*, pp. 443–448, Munich, Germany.
- LUNDBLADH, A., BERLIN, S., SKOTE, M., HILDINGS, C., CHOI, J., KIM, J. & HENNINGSON, D.S. 1999 An efficient spectral method for simulation of incompressible flow over a flat plate. *Tech. Rep.* 1999:11. KTH, Stockholm.
- MALIK, M. R., ZANG, T. A. & HUSSAINI, M. Y. 1985 A spectral collocation method for the Navier-Stokes equations. *J. Comp. Physics* **61**, 64–88.
- SCHLATTER, P., ÖRLÜ, R., Q. LI, G. BRETHOUWER, FRANSSON, J.H.M., JOHANSSON, A.V., ALFREDSSON, P.H & HENNINGSON, D.S. 2009 Turbulent boundary layers up to $Re_\theta = 2500$ studied through simulation and experiment. *Phys. Fluids* **21**, 051702.
- SCHLICHTING, H. & GERSTEN, K. 2003 *Boundary Layer Theory*, 8th edn. Springer.
- SCHNEIDER, K., FARGE, M., PELLEGRINO, G. & ROGERS, M. 2005 Coherent vortex simulation of three-dimensional turbulent mixing layers using orthogonal wavelets. *J. Fluid Mech.* **534**, 39–66.
- SCHNEIDER, K. & VASILYEV, O. 2010 Wavelet methods in computational fluid dynamics. *Annu. Rev. Fluid Mech.* **42**, 473–503.
- SIMENS, M. P., JIMENEZ, J., HOYAS, S. & MIZUNO, Y. 2009 A high-resolution code for turbulent boundary layers. *J. Comput. Phys.* **228**, 4218–4231.
- SKOTE, M. 2001 Studies of turbulent boundary layer flow through direct numerical simulation. PhD thesis, Royal Institute of Technology (KTH), Stockholm, Sweden.
- SPALART, P.R. 1988 Direct simulation of a turbulent boundary layer up to $Re_\theta = 1410$. *J. Fluid Mech.* **187**, 61–98.
- THEODORSEN, T. 1952 Mechanism of turbulence. In *Proc. 2nd Midwestern Conf. Fluid Mech.*. Ohio State University, Columbus, OH.
- WELLER, T., SCHNEIDER, K., OBERLACK, M. & FARGE, M. 2006 DNS and wavelet analysis of a turbulent channel flow rotating about the streamwise direction. In *Turbulence, Heat and Mass Transfer 5* (eds. K. Hanjalic, Y. Nagano & S. Jarkirlic), vol. 1, pp. 163–166.
- WU, X. & MOIN, P. 2009 DNS statistics data of zero-pressure-gradient flat-plate boundary layer. *J. Fluid Mech.* **630**, 5–41.